Scripta Materialia 252 (2024) 116236

Contents lists available at ScienceDirect

Scripta Materialia

journal homepage: www.journals.elsevier.com/scripta-materialia

A novel low-density and high-strength Fe-Ni-base high-entropy superalloy with stable γ/γ' coherent microstructure at 1023 K

Chao Liu [a], Yancheng Li [a], Jinlin Li [a], Zhenhua Wang [a], Qing Wang [a,*], Chuang Dong [a], Peter K. Liaw [b]

[a] School of Materials Science and Engineering, Engineering Research Center of High Entropy Alloy Materials (Liaoning Province), Dalian University of Technology, Dalian 116024, China
[b] Department of Materials Science and Engineering, The University of Tennessee, Knoxville, TN 37996, USA

ARTICLE INFO

Keywords:
Fe-Ni-base superalloys
High-entropy alloying
Microstructural stability
Coherent precipitation
Mechanical property

ABSTRACT

The present work developed a novel low-density (7.71 g/cm^3) and high-strength Fe-Ni-base high-entropy superalloy with a composition of Fe-33.2Ni-13.4Co-13.8Cr -3.1Al-2.2Ti-1.1Nb-1.7Mo-0.03C-0.015B-0.03Zr (wt. %), which contains spherical γ' nanoparticles coherently-precipitated into FCC-γ matrix. These γ' nanoprecipitates were coarsened slowly at 1023 K with the particle size being ~40 nm after 1000 h-aging, showing a great microstructural stability due to lower lattice misfit between γ/γ'. Thus, this superalloy exhibits excellent mechanical properties at room and high temperatures, as evidenced by the yield strength being 743 MPa at 1023 K. The involved strengthening mechanisms were further discussed. Moreover, it has a superior creep-resistant property with the rupture lifetime of 61.5 h under 450 MPa/973 K. Also, it possesses a prominent strain-hardening capacity due to the presence of abundant stacking faults in γ' nanoprecipitates. The current work opens a new way to design low-density superalloys with stable coherent microstructure at high temperatures.

The development of advanced structural materials with prominent mechanical properties and high microstructural stability at high temperatures (HTs), as well as low-density and low-cost, has gained great importance to meet the growing demands for engineering applications in the aerospace field [1–3]. Among them, Ni-base wrought superalloys have been widely used due to their excellent HT mechanical properties and microstructural stability, which mainly benefits from their unique coherent microstructure with spherical or cuboidal $L1_2$-γ' (cubic-Cu_3Au type) nanoparticles precipitated into the face-centered-cubic (FCC)-γ matrix [4–6]. For example, the well-known IN718Plus superalloy (Ni-9.2Fe-9.3Co-17.4Cr-2.7Mo-5.3Nb-0.97Ti-1.6Al-1.19W, wt. %) exhibits a higher yield strength with σ_{YS} ~ 780 MPa at 973 K [7]. However, its long-term service capability at 1023 K is limited owing to the rapid coarsening of γ' nanoprecipitates at this temperature [8]. By contrast, the IN740H superalloy (Ni-19.9Co-25.6Cr-1.5Nb-0.5Mo-1.4Ti-1.5Al) can be endured a long-time (3000 h) aging at 1023 K, exhibiting a high microstructural stability with an extremely-low particle coarsening rate and a relatively-high strength (σ_{YS} ~ 630 MPa at 1023 K) [9]. In order to further enhance the strength, several superalloys containing a high amount of heavy elements have been developed [10–12], but they generally suffer from high density and high cost, such as U720Li (Ni-15Co-16Cr-1.25W-3.0Mo-2.5Al-5Ti) with a density of ~ 8.22 g/cm^3 [12,13]. Thus, it is of great significance to explore novel superalloys with low density, high strength, and high microstructural stability at HTs, which needs to match multiple alloying elements simultaneously and appropriately. However, an inappropriate addition among alloying elements always induces the precipitation of brittle phases, such as σ-(Cr,Mo)(Ni,Co) ($D8_b$-CrFe type) and η-Ni_3Ti ($D0_{24}$-Ni_3Ti type), which can destabilize the γ/γ' coherent microstructure and then deteriorate the HT mechanical property [14–16].

Up to now, many design methods, like *d*-electron theory [17], CALPHAD-aided design [18–20], machine learning (ML) [21], and high-entropy alloying principle [22–25], etc., have been extensively applied to guide the composition design of superalloys. Among them, the high-entropy alloying principle is prevalent since the equimolar or near-equimolar mixing of multi-principal elements in alloys can enhance the structural stability and induce the sluggish effect, which expands traditional alloy-design strategies and provides an enormous composition space to achieve high-performance alloys [22–25]. For instance, the high-entropy γ'-$(Ni,Co,Fe)_3(Al,Ti)$ nanoparticles are

* Corresponding author.
E-mail address: wangq@dlut.edu.cn (Q. Wang).

https://doi.org/10.1016/j.scriptamat.2024.116236
Received 31 March 2024; Received in revised form 8 June 2024; Accepted 13 June 2024
Available online 21 June 2024

coherently-precipitated into the high-entropy FCC-NiCoFe matrix in NiCoFeAlTi system with an equi-molar mixing among elements, which leads to a more stable coherent microstructure at 873 K due to the entropy-increase effect [26,27]. However, it is difficult to balance the addition of oxidation-resistant Cr element with the Fe in these design methods, since the co-addition of Fe and Cr can remarkably destabilize the γ/γ' microstructure at HTs via the brittle phase precipitation [28]. In light of the chemical short-range orders in solid solution structure for describing the local distribution of solute atoms, we proposed the cluster formula approach (i.e., the cluster-plus-glue-atom model) to understand the interactions among alloying elements and the matrix [29]. It is constituted of the nearest-neighbor cluster centered by a solute atom that has a strong interaction with the base atoms and the second-nearest-neighbor atoms to fill into the glue sites among clusters for balancing the atomic-packing density [30]. Then we applied this approach to analyze the composition rule of Ni-base superalloys and found that alloy compositions with optimum properties satisfy the ideal cluster formula of $[\overline{Al}\text{-}\overline{Ni}_{12}]\ (\overline{Al}, \overline{Cr})_3$, in which $\overline{Ni}$, $\overline{Al}$ and $\overline{Cr}$ represent the Ni series of basic elements (Ni, Co, Fe), Al series of γ'-forming elements (Al, Ti, Nb, Ta), and Cr series of soluble elements (Cr, Mo, W), respectively [31]. Based on which, we attempt to introduce a relatively-large amount of Fe to substitute for the base Ni for reducing the density, in which a small amount of Co is also added to improve the matrix stability and to decrease the stacking fault energy. Since a large ratio of Al/(Ti+Nb) (> 0.85 in molar fraction) can avoid brittle phase precipitation, the atom number of (Ti, Nb) in the glue site is determined as 0.5 to get a larger ratio of Al/(Ti+Nb) = 2.0 for a more stable coherent microstructure when Al_1 occupies the cluster center [32]. Accordingly, the atom number of (Cr, Mo) is 2.5 because the total number of glue atoms is 3.0 in the cluster formula. Therefore, the cluster formula of $[Al\text{-}Fe_5Ni_5Co_2](Ti,Nb)_{0.5}(Cr,Mo)_{2.5}$ will be determined to modulate the matching among alloying elements for preventing the brittle phase precipitation from the matrix. Also, a trace amount of C, B, and Zr elements will be added to refine the grain size of matrix and to strengthen the grain boundaries (GBs) [7,33]. Finally, the composition of this superalloy is Fe-33.2Ni-13.4Co-3.1Al-2.2Ti-1.1Nb-13.8Cr-1.7Mo-0.03C-0.015B-0.03Zr (wt. %), possessing a relatively-high configurational entropy ($\Delta S_{conf} = 1.61R$) and a much lower density of $\rho = 7.71$ g/cm^3. The microstructural evolution of coherent γ/γ' phases with the aging time at 1023 K will be investigated, in which the coarsening behavior of γ' nanoprecipitates is involved. Then, the mechanical properties of the superalloy at room temperature (RT) and HTs (973 ~ 1023 K) as well as the creep properties will be measured, where both the strengthening and deformation mechanisms are discussed.

The designed alloy ingot with a weight of ~ 100 g was prepared by vacuum-arc melting under argon atmosphere, in which the purities of raw metals are 99.99 wt. %. The alloy ingot was melted at least five times to ensure composition homogeneity. Alloy ingots were homogenized at 1473 K for 4 h, followed by cold rolling into plates with a total thickness reduction of ~ 85 %. Then these plates were solutionized at 1273 K for 15 mins and subsequently aged at 1023 K for 24 ~ 1000 h. Each heat treatment was followed by water-quenching cooling. A Bruker D8 X-ray diffractometer (XRD) with the Cu K_α radiation (λ = 0.15406 nm) was used to analyze the crystalline structure of designed alloy. The microstructures were examined employing electron backscattered diffraction (EBSD) and IT800-SHL scanning electron microscopy (SEM). The morphology and phase verification were further analyzed by JEM2100FFEG transmission electron microscope (TEM). The statistical

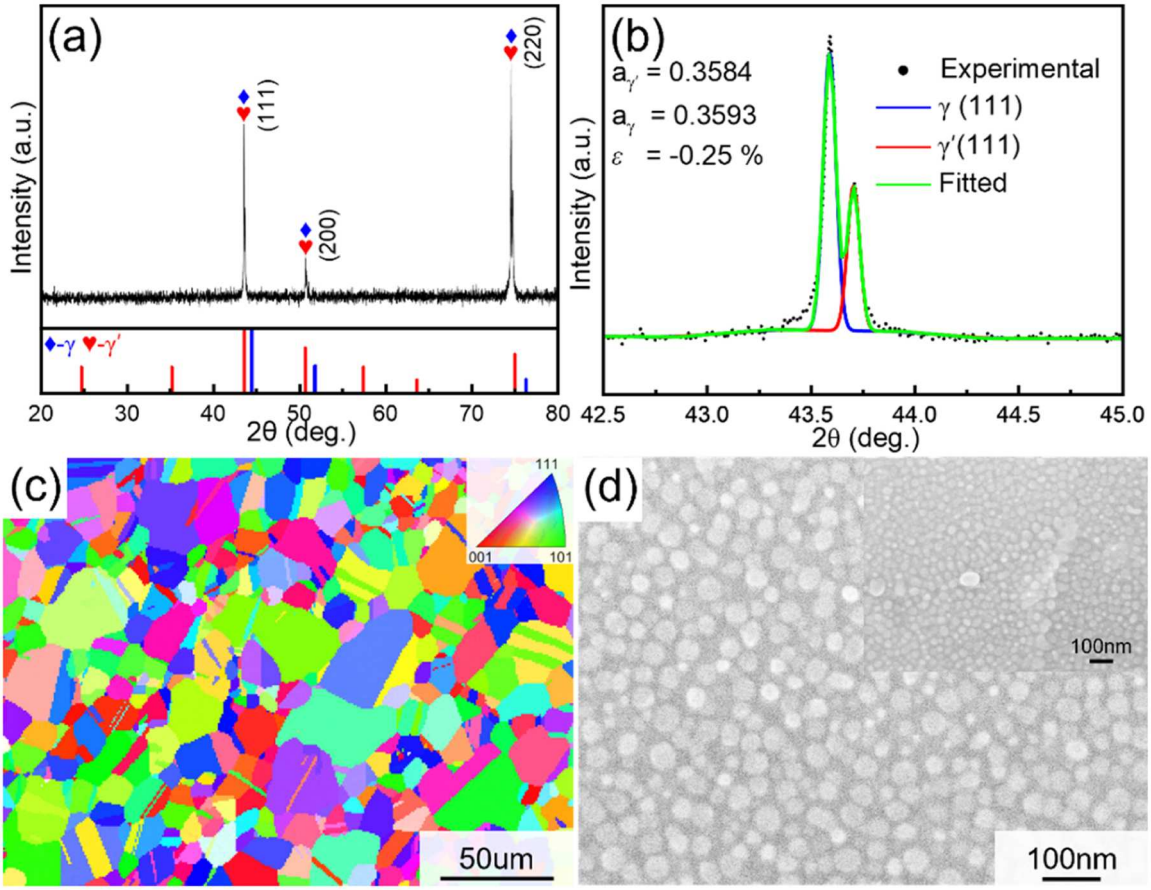

Fig. 1. Phase constitution and microstructural observations of the 24 h-aged alloy. (a, b): XRD patterns, in which the typical peak-separation fitting of primary (111) diffraction peak was shown; (c): EBSD mapping to show an equiaxed microstructure; and (d): SEM-SE observation to show the γ' nanoparticles both in the matrix and on GBs.

analysis of the volume fraction and size of precipitates were measured from the SEM/TEM images (at least 5 images) using the ImageJ software [34]. Uniaxial tensile tests were conducted on a UTM5504 Material Test System at both RT and HTs (973 K and 1023 K). Constant load creep tests were conducted on the current alloy using the RD-50 creep testing machine with a high applied stress of 450 MPa at 973 K. Detailed experimental details are given in the N Y materials.

The XRD result in Fig. 1(a) shows that the 24 h-aged alloy consists of FCC-γ phase and ordered $L1_2$-γ' phase. Since the γ and γ' phases are coherent, their main diffraction peaks are overlapped, where the (111) peak can be separated into two sub-peaks using the pseudo-Voigt function (Fig. 1(b)). Thus, the lattice constants of γ and γ' were obtained as a_γ= 0.3593 nm and $a_{\gamma'}$ = 0.3584 nm. Then the lattice misfit between them was calculated with the equation of $\varepsilon = 2(a_{\gamma'} - a_\gamma)/(a_{\gamma'} + a_\gamma)$ [35], being $\varepsilon \sim$ -0.25 %. The corresponding EBSD result (Fig. 1(c)) shows a fully equiaxed microstructure with the grain size of $d = 19 \pm 6$ μm. The SEM secondary-electron (SE) image (Fig. 1(d)) indicates that spherical γ' nanoparticles are uniformly distributed in the FCC-γ matrix, with the particle size and volume fraction being $r = 16 \pm 3$ nm and $f = 38.4 \pm 1.7$ %, respectively. In addition, no other phases were found on GBs in this state, besides the partially-coarsened γ' nanoprecipitates (the inset of Fig. 1(d))

In order to study the thermal stability of γ/γ' coherent microstructure, alloy specimens were isothermally aged at 1023 K for a long time

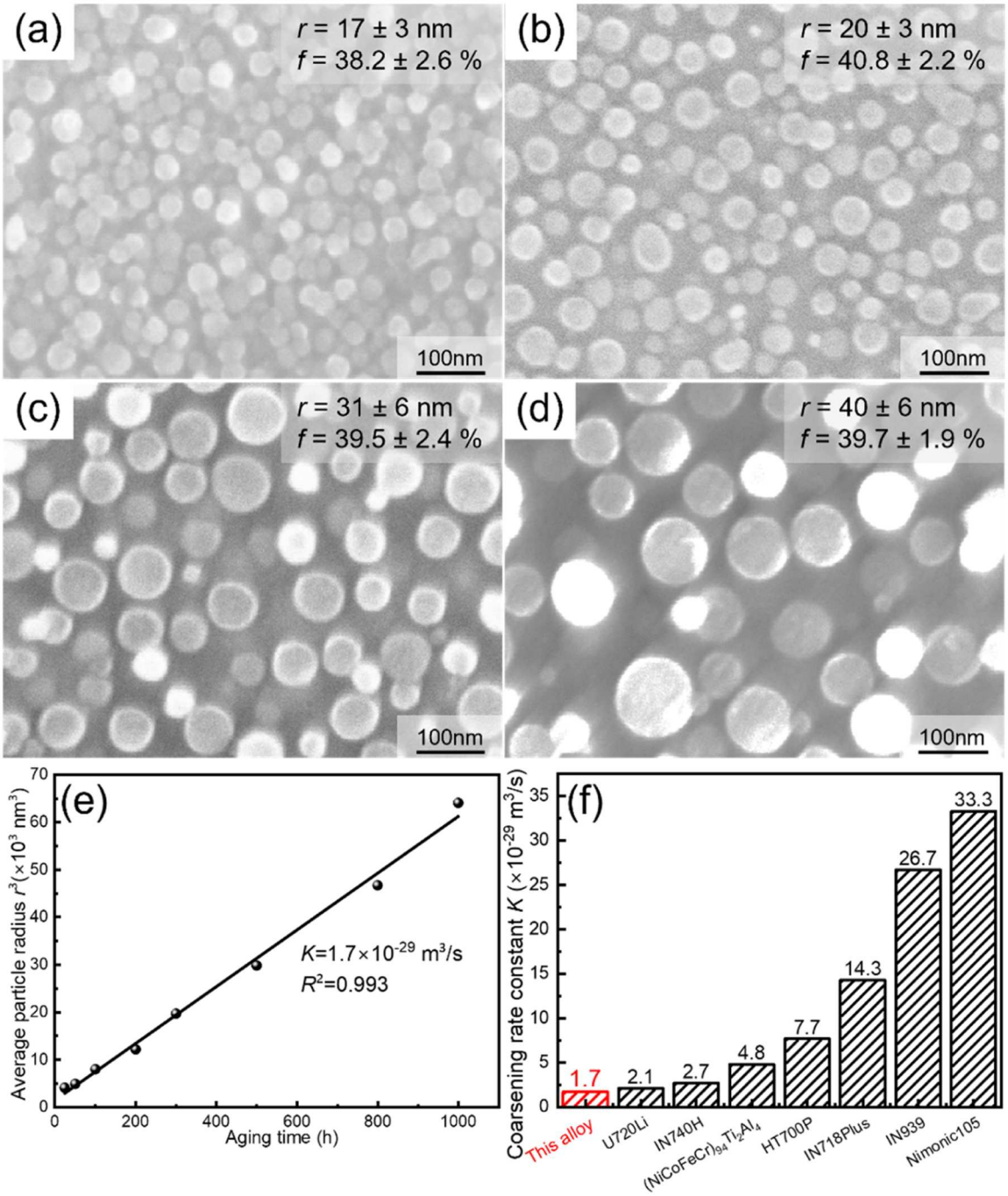

Fig. 2. SEM-SE observations of the designed alloy after aging at 1023 K for 50 h (a), 100 h (b), 500 h (c), and 1000 h (d). (e): Variation of the average particle radius r^3 of γ' precipitates with aging time, in which the fitted coarsening rate constant K of particles was fitted and the coefficient of determination R^2 was also marked; (f): Comparison of the K value in this alloy with those in reported typical alloys at 1023 K.

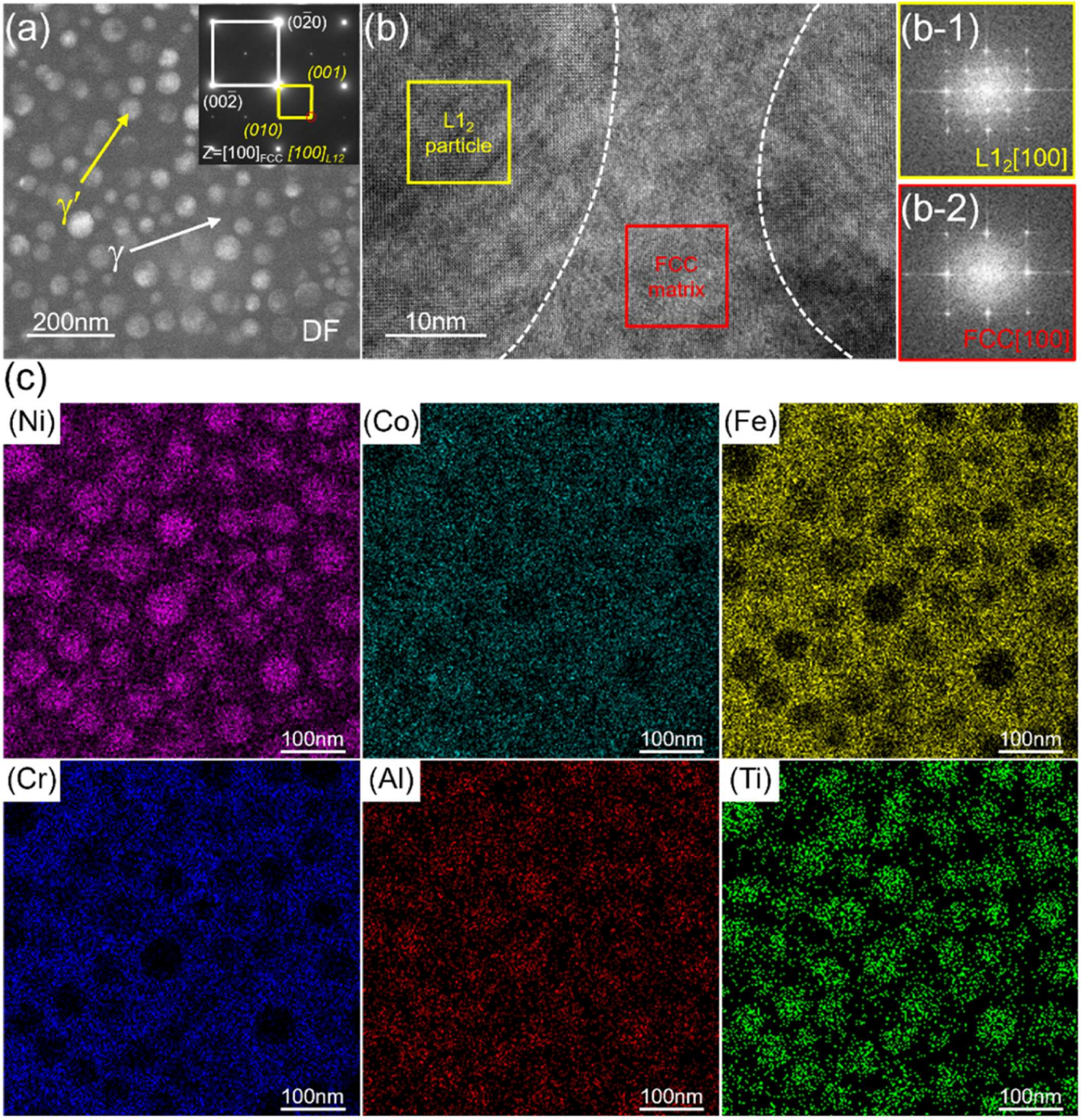

Fig. 3. TEM characterization of the 500 h-aged alloy. (a): DF-TEM image and corresponding SAED pattern; (b): HRTEM image to show the coherent interfaces between γ/γ', where the FFT patterns were obtained from γ' nanoparticle (b-1) and γ matrix (b-2); and (c): Elemental distributions in coherent γ/γ' microstructure mapped with TEM-EDS.

up to 1000 h, and the SEM-SE observations are shown in Fig. 2. It can be seen that these spherical γ' nanoparticles are coarsened slowly with the aging time, as evidenced by the fact that the particle size increases from $r = 17 \pm 3$ nm in 50 h-aged state to $r = 31 \pm 6$ nm in 500 h-aged state, and then to $r = 40 \pm 6$ nm in 1000 h-aged state. During this process, the particle morphology is not changed and the volume fraction keeps almost constant, being $f \sim 39$ %. It is consistent with the classical Philippe-Voorhees (PV) theory, i.e., the coherent precipitates in multi-component alloys are generally coarsened by the agglomeration of precipitates during aging without any change in volume fraction [36]. Thus, the time-dependent coarsening process of γ' nanoprecipitates in the current alloy can be described by Eq. (1) [36]:

$$r(t)^3 - r(t_0)^3 = K(t - t_0) \quad (1)$$

where r(t) is the average particle radius at the aging time t; $t_0 = 24$ h is the starting time for γ' coarsening; and K is the coarsening rate constant of precipitates. Fig. 2(e) gives the variation of particle size (r^3) with the aging time, which can be well fitted by the PV theory. Thus, the coarsening rate constant of γ' precipitates is evaluated as $K = 1.7 \times 10^{-29}$ m^3/s at 1023 K. It is much lower than those of reported typical superalloys and high-entropy alloys (HEAs) at the same temperature [8,9,37–40], as seen in Fig. 2(f), such as IN718Plus ($K = 14.3 \times 10^{-29}$ m^3/s) [7]. And it is comparable to those of IN740H and U720Li with an extremely-low K values ($2.1 \sim 2.7 \times 10^{-29}$ m^3/s) [9,40] and $(NiCoFeCr)_{94}Ti_2Al_4$ HEA ($K = 4.8 \times 10^{-29}$ m^3/s) [37], which indicates that the current alloy has a much more stable γ/γ' coherent microstructure. In fact, the slow coarsening of γ' particles is mainly ascribed to the smaller lattice misfit between γ/γ', which remains almost unchanged (ε = -0.25 ~ -0.27 %) during the aging process, as seen in Fig. S1 of Supplementary Materials.

The 500 h-aged alloy was further characterized by TEM, as seen in Fig. 3. Both the TEM dark-field (DF) image and the selected area electron diffraction (SAED) pattern along the $[100]_{FCC}$ direction (Fig. 3(a)) show that spherical γ' nanoparticles are precipitated into the FCC-γ matrix. The particle size and volume fraction of γ' nanoprecipitates in this state are $r = 31 \pm 5$ nm and $f = 37.2 \pm 2.2$ %, respectively, which is in a good consistence with the SEM results. In addition, the high-resolution TEM (HRTEM) image and the corresponding fast Fourier transformation (FFT) patterns in Fig. 3(b, b-1, b-2) indicate that the interfaces (marked with white dashed lines) between γ' nanoparticles and γ matrix are coherent. Also, the elemental distributions in the γ/γ' coherent microstructure were analyzed using the TEM-EDS (Fig. 3(c)), from which it is found that the Ni, Al, and Ti elements are obviously enriched in the γ' nanoparticles, while the Fe, Co, and Cr elements are mainly segregated in the FCC-γ matrix.

The tensile engineering stress-strain curves of the current alloy in different aged states at RT and HTs are presented in Fig. 4(a). It is found that the yield strength values at RT keep almost constant with the aging time, being $\sigma_{YS} = 852$ MPa in 24 h-aged state, $\sigma_{YS} = 894$ MPa in 100 h-aged state, $\sigma_{YS} = 859$ MPa in 200 h-aged state, and $\sigma_{YS} = 866$ MPa in 500 h-aged state, which is mainly derived from the stable γ/γ' coherent microstructure. In addition, this alloy has a good ductility with the elongation of ~ 20 %. More importantly, the current alloy has a much higher strength at HTs, being $\sigma_{YS} = 788$ MPa at 973 K and $\sigma_{YS} = 743$ MPa at 1023 K. Fig. 4(b) compares the specific yield strength with the temperature of this alloy with those of existing superalloys [7,9,40–45]. Significantly, the specific strength of the alloy at 1023 K (96.4 MPa/(g•cm^{-3})) is superior to those of superalloys, such as IN718Plus (75.4 MPa/(g•cm^{-3})) [7] and IN740H (77.9 MPa/(g•cm^{-3})) [9]. Furthermore, the strength of the current alloy is not sensitive to the temperature from RT to 1023 K, showing an extremely-slow reduction tendency compared with those in existing superalloys. Additionally, Fig. 4(c) plots the variation of the creep strain with the time under the condition of 450 MPa / 973 K for the 24 h-aged alloy, from which the measured creep rupture lifetime is 61.5 h. Fascinatingly, the rupture lifetime of this alloy is about 4 times larger than that (13 h) of the commercial A286 Fe-Ni-base superalloy (Fe-24.6Ni-14.7-Cr-0.16Al-2.2Ti-1.23Mo, wt. %) [45], and 3 times larger than that (22 h) of $Ni_{29.9}Co_{30}Fe_{13}Cr_{15}Al_6Ti_6B_{0.1}$ (at.%) HEA [46] under the same condition, as presented in Fig. 4(d), indicating that the current alloy has a superior creep property.

In order to better understand the high strength of the current alloy, the classical strengthening mechanisms at RT were employed. Thus, the contributions to the yield strength of this alloy mainly derive from three strengthening mechanisms, i.e., $\sigma_{YS} = \Delta\sigma_{ss} + \Delta\sigma_G + \Delta\sigma_p$, where the $\Delta\sigma_{ss}$, $\Delta\sigma_G$, and $\Delta\sigma_p$ are the strength increments from the solid-solution strengthening, grain-boundary strengthening, and precipitation strengthening of γ' particles, respectively [47]. The calculation details using the 500 h-aged specimen as an example are presented in Supplementary Materials. The calculated strength increments are $\Delta\sigma_{ss} = 169$ MPa, $\Delta\sigma_G = 52$ MPa, and $\Delta\sigma_p = 633$ MPa, leading to a total sum of $\sigma_{YS} = 169 + 52 + 633 = 854$ MPa (Fig. 4(a)), which matches well with the experimental value of 866 MPa. Obviously, the precipitation strengthening mechanism plays a dominant role in the designed alloy.

Interestingly, this alloy exhibits an excellent strain-hardening capacity, as evidenced by a much higher ratio of ultimate tensile strength to yield strength ($\sigma_{UTS}/\sigma_{YS} \sim 1.45$). Fig. 4(e) shows the strain-hardening behavior for the current alloy as a function of the true strain. It exhibits a steady uniform plastic deformation within the strain range of 4 ~ 15 %, leading to a continuous increase in the tensile strength up to 1240 MPa. Then the uniformly-deformed microstructure of 500 h-aged sample after tension was observed with TEM under two-beam conditions, as seen in Fig. 4(f), from which it can be found that large amounts of dislocations are accumulated in both FCC matrix and γ' nanoparticles. And, dislocations cut through these fine γ' nanoparticles during the slipping process, which is consistent with the precipitation strengthening induced by the dislocation shearing mechanism. Moreover, abundant stacking faults (SFs) also occur in the γ/γ' coherent microstructure (Fig. 4(g)), which is mainly due to the relatively-lower stacking fault energy (< 50 mJ/m^2) induced by the introduction of Co [48–50]. Actually, this phenomenon of SFs shearing the γ' nanoparticles always appears in Co-containing superalloys, which results in the formation of superlattice intrinsic stacking faults, as presented in Fig. 4(h). It is known that the formation and refinement of SFs could effectively prevent the movement of dislocations, which decreases the mean free path of dislocations and then produces a dynamic Hall-Petch effect remarkably [28]. Therefore, the dislocation slip and the formation of SFs are the main deformation mechanisms of the current alloy, which contributes to the pronounced strain-hardening capability.

In conclusion, a novel Fe-Ni-base high-entropy superalloy (Fe-33.2Ni-13.4Co-3.1Al-2.2Ti-1.1Nb-13.8Cr-1.7Mo-0.03C-0.015B-0.03Zr wt. %) with γ/γ' coherent precipitation and low density ($\rho = 7.71$ g/cm^3) was developed in light of the cluster formula approach. It exhibits a much higher γ/γ' microstructural stability at 1023 K, as evidenced by the fact that the particle size of γ' nanoparticles changes from ~16 nm in 24 h-aged state to ~40 nm in 1000 h-aged state. The extremely-slow coarsening behavior of γ' nanoprecipitates, characterized by the coarsening rate constant ($K = 1.7 \times 10^{-29}$ m^3/s), is mainly attributed to a lower lattice misfit (~ -0.25 %) between γ/γ'. Meanwhile, the stable coherent microstructure renders the current alloy with high strength ($\sigma_{YS} = 852$ MPa at RT, $\sigma_{YS} = 743$ MPa at 1023 K) and prominent creep-resistant property (the rupture lifetime of 61.5 h under the condition of 450 MPa / 973 K). Moreover, this superalloy also exhibits a prominent strain-hardening capacity, which is ascribed to both the dislocation slip in the matrix and the formation of a large amount of stacking faults in γ' nanoparticles.

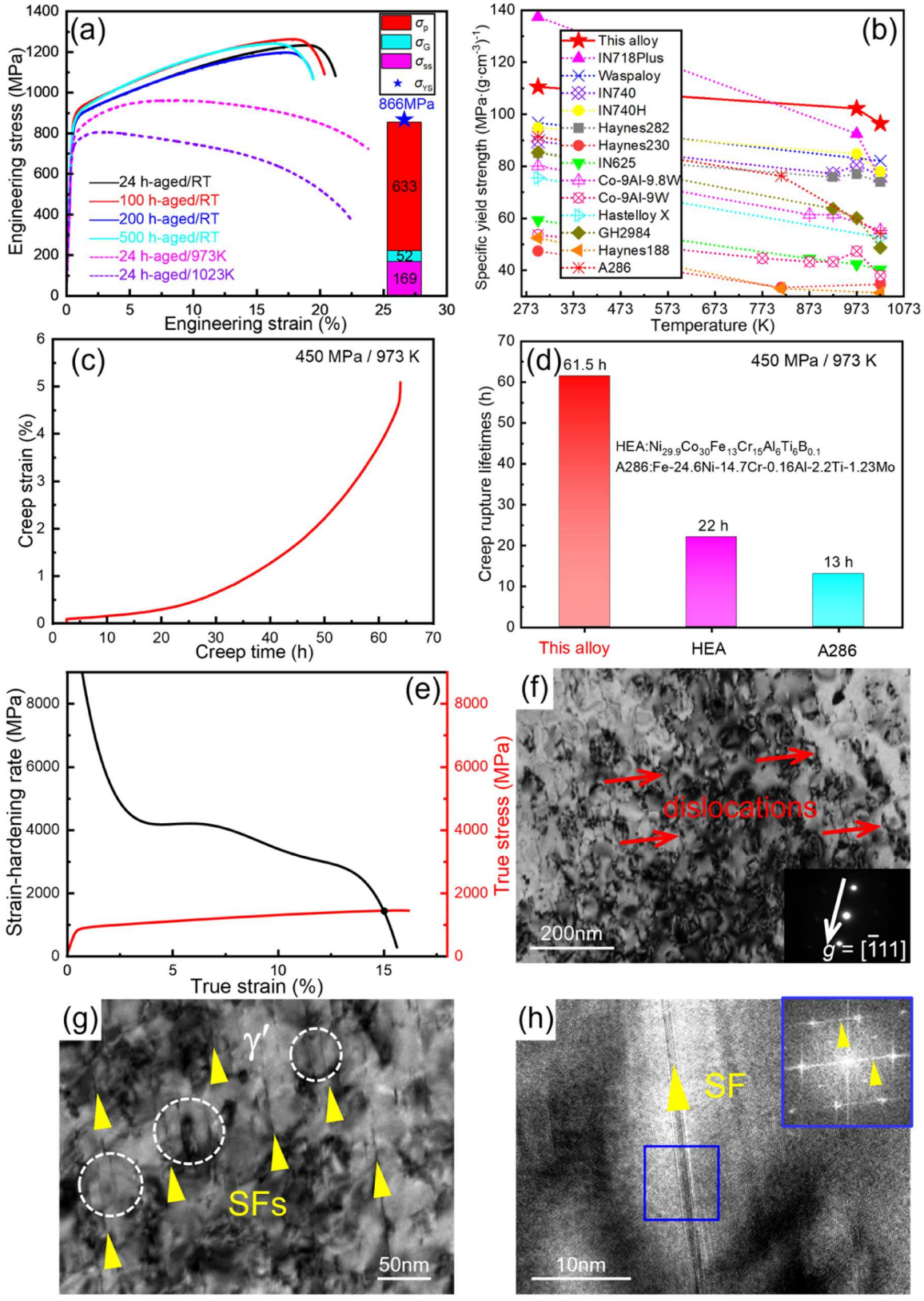

Fig. 4. (a): Mechanical properties of the current alloy in different aged states; (b): Comparison of the variation of specific yield strength with temperature of the current alloy with those of existing superalloys; (c): Creep curve of the current alloy under the condition of 450 MPa / 973 K; (d): Comparison of creep properties of the current alloy with other alloys. (e): True stress-strain curves and the corresponding strain hardening rate curves of the current alloy; (f): BF-TEM images of 500 h-aged alloy after tension under two-beam conditions, which is close to [110] axis; (g, h): BF-TEM images, HRTEM image and corresponding FFT pattern of 500 h-aged alloy after tension along [110] axis.

CRediT authorship contribution statement

Chao Liu: Writing – original draft, Visualization, Methodology, Investigation, Formal analysis, Data curation. **Yancheng Li:** Writing – original draft, Methodology, Investigation. **Jinlin Li:** Writing – original draft, Methodology, Investigation. **Zhenhua Wang:** Visualization, Methodology, Investigation. **Qing Wang:** Writing – review & editing, Validation, Supervision, Resources, Funding acquisition, Conceptualization. **Chuang Dong:** Supervision, Methodology, Conceptualization. **Peter K. Liaw:** Writing – review & editing, Resources, Funding acquisition, Conceptualization.

Declaration of competing interest

The authors declare that they have no known competing financial interests or personal relationships that could have appeared to influence the work reported in this paper.

Acknowledgements

It was supported by the National Natural Science Foundation of China (52171152). P. K. Liaw very much appreciates the support from the National Science Foundation (DMR-1611180, 1809640, and 2226508) and the Army Research Office (FA9550-23-1-0503, W911NF-13-1-0438, and W911NF-19-2-0049). The authors thank F.Y. Yu at the Dalian University of Technology for help with SEM/EBSD characterization and analysis.

Supplementary materials

Supplementary material associated with this article can be found, in the online version, at doi:10.1016/j.scriptamat.2024.116236.

References

[1] R.C. Reed, The Superalloys Fundamentals and Applications, Cambridge University Press, 2006.
[2] X.S. Zhang, Y.J. Chen, J.L. Hu, Recent advances in the development of aerospace materials, Prog. Aerosp. Sci. 97 (2018) 22–34.
[3] J. Joseph, M. Annasamy, P. Cizek, A. Vahid, P.D. Hodgson, M.R. Barnett, D. M. Fabijanic, Design of precipitation (γ') strengthened Fe-rich medium entropy alloys, Scr. Mater. 235 (2023) 115630.
[4] E. Nembach, G. Neite, Precipitation hardening of superalloys by ordered γ'-particles, Prog. Mater. Sci. 29 (1985) 177–319.
[5] Z.R. Yan, K. Srikakulapu, Y. Gao, H.L. Qin, Y. Rong, Z.N. Bi, Q.G. Xie, K. An, Y. D. Wang, Q. Tan, γ'-size effect on the deformation microstructure and texture in a Ni-based superalloy using *in-situ* neutron diffraction, Scr. Mater. 236 (2023) 115665.
[6] A. Harte, M. Atkinson, A. Smith, C. Drouven, S. Zaefferer, J.Q.D. Fonseca, M. Preuss, The effect of solid solution and gamma prime on the deformation modes in Ni-based superalloys, Acta Mater. 194 (2020) 257–275.
[7] S.A. Hosseini, S.M. Abbasi, K.Z. Madar, The effect of boron and zirconium on microstructure and tensile properties of the wrought nickel-based superalloy ATI 718Plus, Mater. Sci. Eng. A 712 (2018) 780–789.
[8] L.T. Tang, Q.Y. Guo, C. Li, R. Ding, Y.C. Liu, Precipitation and tensile behaviors of Allvac 718Plus superalloy during long-term thermal exposure, Mater. Sci. Eng. A 896 (2024) 146221.
[9] Y. Chong, Z.D. Liu, G. Andy, W. Liu, Y.Q. Weng, Microstructure evolution and mechanical properties of Inconel 740H during aging at 750°C, Mater. Sci. Eng. A 589 (2014) 153–164.
[10] D.F. Shi, Z.J. Zhang, Y.H. Yang, Y.Z. Zhou, R. Liu, P. Zhang, Z.F. Zhang, High-temperature fatigue strength of grain boundaries with different misorientations in nickel-based superalloy bicrystals, J. Mater. Sci. Technol. 154 (2023) 94–106.
[11] L.L. Zhu, X. Yu, W.F. Li, L.N. Zhang, N.X. Zhang, Y.N. Lv, L. Zhao, W.Y. Zhang, Z. Wang, H.Y. Yu, Z.N. Bi, H. Han, J.J. Ruan, L. Jiang, High-throughput investigation of Nb and Ta alloying effects on the microstructure and properties of a novel Ni-Co-based superalloy, Scr. Mater. 226 (2023) 115215.
[12] A.A.N. Németh, D.J. Crudden, D.E.J. Armstrong, D.M. Collins, K. Li, A. J. Wilkinson, C.R.M. Grovenor, R.C. Reed, Environmentally-assisted grain boundary attack as a mechanism of embrittlement in a nickel-based superalloy, Acta Mater. 126 (2017) 361–371.
[13] B.D. Conduit, N.G. Jones, H.J. Stone, G.J. Conduit, Design of a nickel-base superalloy using a neural network, Mater. Des. 131 (2017) 358–365.
[14] C.M.F. Rae, R.C. Reed, The precipitation of topologically close-packed phases in rhenium-containing superalloys, Acta Mater. 49 (2001) 4113–4125.
[15] T. Yang, Y.L. Zhao, L. Fan, J. Wei, J.H. Luan, W.H. Liu, C. Wang, Z.B. Jiao, J.J. Kai, C.T. Liu, Control of nanoscale precipitation and elimination of intermediate-temperature embrittlement in multicomponent high-entropy alloys, Acta Mater. 189 (2020) 47–59.
[16] B. Seiser, R. Drautz, D.G. Pettifor, TCP phase predictions in Ni-based superalloys: structure maps revisited, Acta Mater. 59 (2011) 749–763.
[17] M. Mostafaei, S.M. Abbasi, Designing and characterization of Al- and Ta-bearing Ni-base superalloys based on d-electrons theory, Mater. Des. 127 (2017) 67–75.
[18] T. Yang, Y.L. Zhao, J.H. Luan, B. Han, J. Wei, J.J. Kai, C.T. Liu, Nanoparticles-strengthened high-entropy alloys for cryogenic applications showing an exceptional strength-ductility synergy, Scr. Mater. 164 (2019) 30–35.
[19] J.W. Yin, Z.Y. Rao, D.Y. Wu, H.P. Lv, H.K. Ma, T. Long, J. Kang, Q. Wang, Y. D. Wang, R. Su, Interpretable predicting creep rupture life of superalloys: enhanced by domain-specific knowledge, Adv. Sci. 11 (2024) 2307982.
[20] J.J. Ruan, W.W. Xu, Y T, J.X. Yu, S.Y. Yang, J.H. Luan, T. Omori, C.P. Wang, R. Kainuma, K. Ishida, C.T. Liu, X.J. Liu, Accelerated design of novel W-free high-strength Co-base superalloys with extremely wide γ/γ' region by machine learning and CALPHAD methods, Acta Mater. 186 (2020) 425–433.
[21] Z.Y. Rao, P.Y. Tung, R.W. Xie, Y. Wei, H.B. Zhang, A. Ferrari, T.P.C. Klaver, F. Körmann, P.T. Sukumar, A.K.D. Silva, Y. Chen, Z.M. Li, D. Ponge, J. Neugebauer, O. Gutfleisch, S. Bauer, D. Raabe, Machine learning-enabled high-entropy alloy discovery, Science 378 (2022) 78–85.
[22] J.W. Yeh, S.K. Chen, S.J. Lin, J.Y. Gan, T.S. Chin, T.T. Shun, C.H. Tsau, S.Y. Chang, Nanostructured high-entropy alloys with multiple principal elements: novel alloy design concepts and outcomes, Adv. Eng. Mater. 6 (2004) 299–303.
[23] D.B. Miracle, O.N. Senkov, A critical review of high entropy alloys and related concepts, Acta Mater. 122 (2017) 448–511.
[24] E.P. George, D. Raabe, R.O. Ritchie, High-entropy alloys, Nat. Rev. Mater. 4 (2019) 515–534.
[25] Y.T. Chen, Y.J. Chang, H. Murakami, S. Gorsse, A.C. Yeh, Designing high entropy superalloys for elevated temperature application, Scr. Mater. 187 (2020) 177–182.
[26] T. Yang, Y.L. Zhao, Y. Tong, Z.B. Jiao, J. Wei, J.X. Cai, X.D. Han, D. Chen, A. Hu, J. J. Kai, K. Lu, Y. Liu, C.T. Liu, Multicomponent intermetallic nanoparticles and superb mechanical behaviors of complex alloys, Science 362 (2018) 933–937.
[27] J.X. Hou, S.F. Liu, B.X. Cao, J.H. Luan, Y.L. Zhao, Z. Chen, Q. Zhang, X.J. Liu, C. T. Liu, J.J. Kai, T. Yang, Designing nanoparticles-strengthened high-entropy alloys with simultaneously enhanced strength-ductility synergy at both room and elevated temperatures, Acta Mater. 238 (2022) 118216.
[28] Z.H. Zhong, Y.F. Gu, Y. Yuan, Microstructural stability and mechanical properties of a newly developed Ni-Fe-base superalloy, Mater. Sci. Eng. A 622 (2015) 101–107.
[29] C. Dong, Z.J. Wang, S. Zhang, Y.M. Wang, Review of structural models for the compositional interpretation of metallicglasses, Int. Mater. 65 (2020) 286–296.
[30] C. Chen, Q. Wang, C. Dong, Y. Zhang, H.G. Dong, Composition rules of Nibase single crystal superalloys and its influence on creep properties via a cluster formula approach, Sci. Rep. 10 (2020) 21621.
[31] J.D. Sun, J.L. Li, H.Y. Yu, Z.H. Wang, Q. Wang, C. Dong, Microstructural stability of low-cost Ni-base superalloys with a high volume fraction of cuboidal γ' nanoprecipitates, Mater. Sci. Eng. A 833 (2022) 142550.
[32] S. Antonov, M. Detrois, R.C. Helmink, S. Tin, Precipitate phase stability and compositional dependence on alloying additions in γ-γ'-δ-η Ni-base superalloys, J. Alloys Compd. 626 (2015) 76–86.
[33] T. Yang, Y.L. Zhao, W.P. Li, C.Y. Yu, J.H. Luan, D.Y. Lin, L. Fan, Z.B. Jiao, W.H. Liu, X.J. Liu, J.J. Kai, J.C. Huang, C.T. Liu, Ultrahigh-strength and ductile superlattice alloys with nanoscale disordered interfaces, Science 369 (2020) 427–432.
[34] C.A. Schneider, W.S. Rasband, K.W. Eliceiri, NIH image to ImageJ: 25 years of image analysis, Nat. Methods 9 (2012) 671–675.
[35] A.B. Parsa, D. Bürger, T.M. Pollock, G. Eggeler, Misfit and the mechanism of high temperature and low stress creep of Ni-base single crystal superalloys, Acta Mater. 264 (2024) 119576.
[36] T. Philippe, P.W. Voorhees, Ostwald ripening in multicomponent alloys, Acta Mater. 61 (2013) 4237–4244.
[37] Y.Y. Zhao, H.W. Chen, Z.P. Lu, T.G. Nieh, Thermal stability and coarsening of coherent particles in a precipitation-hardened $(NiCoFeCr)_{94}Ti_2Al_4$ high-entropy alloy, Acta Mater. 147 (2018) 184–194.
[38] Y.S. Huang, R. Zhang, Z.J. Zhou, J.B. Yan, Y. Yuan, Y.F. Gu, C.Y. Cui, Y.Z. Zhou, X. F. Sun, Effect of long-term aging on microstructural stability and tensile deformation of a Fe-Ni-based superalloy, Mater. Sci. Eng. A 847 (2022) 143298.
[39] P.K. Footner, B.P. Richards, Long-term growth of superalloy γ' particles, J. Mater. Sci. 17 (1982) 2141–2153.
[40] B. Geddes, H. Leon, X. Huang, Superalloys: Alloying and Performance, ASM International, 2010.
[41] Z.L. Huang, Z.R. Zhai, W.H. Lin, H. Chang, Y.N. Wu, R. Yang, Z.B. Zhang, On the orientation dependent microstructure and mechanical behavior of Hastelloy X superalloy fabricated by laser powder bed fusion, Mater. Sci. Eng. A 844 (2022) 143208.
[42] Z.Y. Dai, Y.H. Su, T.S. Yang, Y.D. Wang, X.W. Liang, Z.Y. Wei, X.W. Zhang, Study on intermediate temperature brittleness mechanism of Inconel 625 deposited metal, J. Mater. Res. Technol. 17 (2022) 1812–1821.
[43] Y.C. Chen, C.P. Wang, J.J. Ruan, T. Omori, R. Kainuma, K. Ishida, X.J. Liu, High-strength Co-Al-V-base superalloys strengthened by γ'-Co3(Al,V) with high solvus temperature, Acta Mater. 170 (2019) 62–74.
[44] F. Sun, Y.F. Gu, J.B. Yan, Z.H. Zhong, M. Yuyama, Tensile deformation-induced dislocation configurations at intermediate temperatures in a Ni-Fe-based superalloy for advanced ultra-supercritical coal-fired power plants, J. Alloys Compd. 657 (2016) 565–569.

[45] H.D. Cicco, M.I. Luppo, L.M. Gribaudo, J.O. Garcia, Microstructural development and creep behavior in A286 superalloy, Mater. Charact. 52 (2004) 85–92.
[46] L.J. Jing, B.X. Cao, Y.X. Wang, J. Wei, T. Yang, Y.L. Zhao, Defeating creep embrittlement under high-stress levels through heterogeneous grain architecture in a $L1_2$-strengthened multicomponent alloy, Mater. Sci. Eng. A 895 (2024) 146223.
[47] A. Argon, Strengthening Mechanisms in Crystal Plasticity, Oxford University Press, 2007.
[48] L. Zhang, Z.H. Hu, L. Zhang, H. Wang, J.B. Li, Z. Li, J.X. Yu, B.L. Wu, Enhancing the strength-ductility trade-off in a NiCoCr-based medium-entropy alloy with the synergetic effect of ultra fine precipitates, stacking faults, dislocation locks and twins, Scr. Mater. 211 (2022) 114497.
[49] W.Q. Guo, J. Su, W.J. Lu, C.H. Liebscher, C. Kirchlechner, Y.J. Ikeda, F. Körmann, X. Liu, Y.F. Xue, G. Dehm, Dislocation-induced breakthrough of strength and ductility trade-off in a non-equiatomic high-entropy alloy, Acta Mater. 185 (2020) 45–54.
[50] Z.B. An, S.C. Mao, C. Jiang, Z.Y. Li, S.C. Wu, Y.D. Zhai, L. Wang, Y.N. Liu, Z. Zhang, X.D. Han, Achieving superior combined cryogenic strength and ductility in a high-entropy alloy via the synergy of low stacking fault energy and multiscale heterostructure, Scr. Mater. 239 (2024) 115809.